JOURNAL OF MATERIALS SCIENCE 31 (1996) 6351–6359

Deformation and fracture of Al–8Fe rapidly solidified alloys

P. ROZENAK
Practical Engineering College of Beer-Sheva, Department of Mechanical Engineering, Ben Gurion University of the Negev, PO Box 45, Beer-Sheva 84100, Israel

The effects of the rapid solidification on the deformation and fracture of Al–8Fe alloys, from TEM fracture specimens, have been studied. The most general conclusion which can be drawn in this study is clearly in agreement with a plastic deformation mechanism. Crack propagation occurs by localized plastic rupture mechanisms which result from enhanced slip along $\{1\,1\,1\}_\gamma$ planes. Crack propagation occurs within the deformed zone either by the nucleation, growth and coalescence of holes ahead of the crack-tip, or through the emission of dislocation from the crack-tip. The resulting fracture is along the active $\{1\,1\,1\}_\gamma$ slip planes. The principal effect of secondary phases ($Al_{13}Fe_4$) on the fracture propagation in Al–8Fe alloys was that the secondary phases increased the stress level at which plastic deformation occurs at the crack-tip and increased the stress level at which the crack propagates. This work clearly shows that in order to obtain coarse intermetallic precipitates in the specimens after ageing heat treatments the crack propagation and deformation processes occur at lower stresses compared to as-received rapidly solidified samples.

1. Introduction

The development of refined microstructures for dispersion strengthening of Al alloys by rapid solidification is related to under cooling at nucleation and during competitive crystal growth. Based on the analysis of solidification, it is possible to obtain metastable structures or suppression of coarse primary intermetallic phases which are useful for the development of dispersoid structures. Strength and stability of Al alloys at elevated temperatures are derived partly from non-equilibrium intermetallic phases produced during solidification and are thus dependent on the thermal stability of such intermetallics [1–4].

The present paper reports on the deformation and fracture experiments of Al–8Fe alloys rapidly solidified as-received and after ageing heat treatments during *in situ* deformation by transmission electron microscopy (TEM) at room temperature. The effects on the dislocation mobility and crack propagation rate are observed directly at high magnification and the mechanism of secondary phases related to crack propagation under mode I applied stresses is more fully specified.

2. Experimental procedure

High purity Al–8Fe alloy ingots were produced by induction melting in an Ar atmosphere. Rapidly solidified ribbons were prepared by a melt-spinning technique [5], at a perisheral wheel at a velocity of 22.4 $m\,s^{-1}$. A melt temperature of 1000 °C was used to ensure complete dissolution. The ribbons produced were typically ca. 25–100 mm thick and 2–4 mm wide. The specimens were aged at 25–500 °C for 2 h under a vacuum of 1.333×10^{-3} Pa. The microstructures were characterized using a Phillips X-ray diffractometer with a step motor and programmer. Both CuK_α and CoK_α radiations were used in this study. Knoop microhardness measurements were made by using a MHT-1, Matsuzava instrument, at a load of 10 g and a d-well time of 10 s. The microhardness values were taken as the mean of five measurements from the polished longitudinal cross-section of various ribbon zones: air side, centre and wheel sides. Optical micrographs of a representative longitudinal cross-section of as-cast rapidly solidified ribbons showed a non-continuous featureless region 10–20 μm wide near to the wheel side, in the centre columnar dendritic region, then an equiaxed region extending to the top of the ribbon [6].

Deformation and fracture studies were carried out by TEM (Jeol 200B; operating at 150 kV) using a single-axis tensile stage designed to introduce tensile stress. Tensile specimens (8×3 mm) were prepared with their long axes. The centre section taken from columnar dendritic zones (for all specimens) were prepared by electrolytic polishing at 10 V in a polishing cell with 200 cm^3 nitric acid and 800 cm^3 methanol at − 18 °C.

3. Results

XRD obtained from the rapidly solidified ribbons indicated formation of secondary intermetallic phases in the solid solution of Al. Diffraction patterns from the secondary phase were readily indexed as $Al_{13}Fe_4$ (Figs 1 and 2, Tables I and II). Low diffraction intensities from the $Al_{13}Fe_4$ phase were obtained after

0022–2461

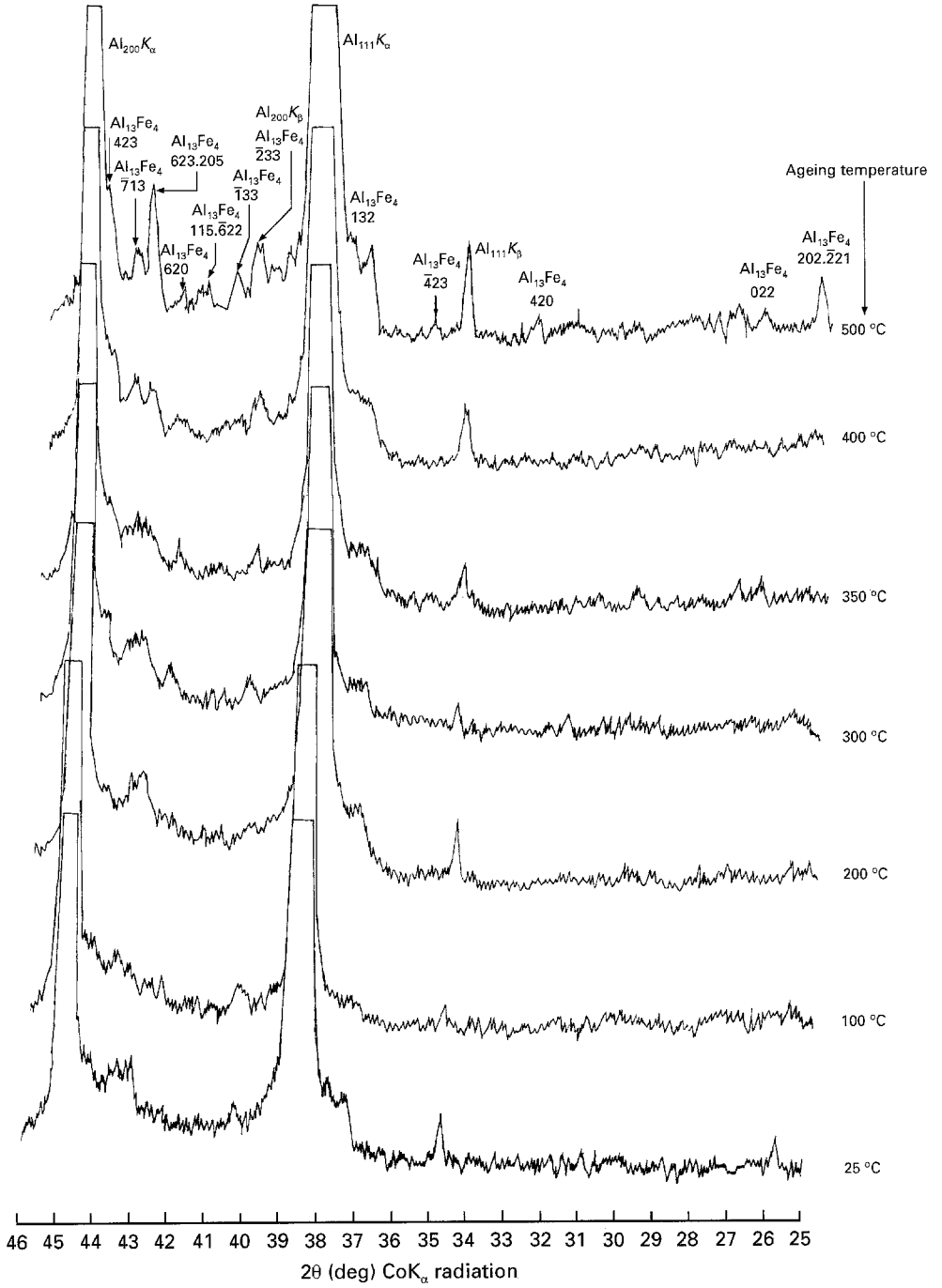

Figure 1 XRD pattern of a rapidly solidified Al–8Fe alloy after isochronal ageing at the indicated temperatures for 2 h.

rapid solidification (Figs 1 and 2). Diffraction intensities from $Al_{13}Fe_4$ increased with an increase in the isochonal ageing temperature. Reflections K_α and K_β obtained from the Al matrix indicated shifts to smaller 2θ values during the ageing process (Figs 1 and 2). Tables I and II summarize the XRD results compared to the powder diffraction standards (PDS) obtained from various radiations of the Al–8Fe alloy rapidly solidified and after isochronal ageing heat treatments.

Microhardness results obtained from the featureless, columnar and equiaxed regions of the rapidly solidified Al–8Fe alloy are shown in Fig. 3. The featureless region indicates the higher hardness values (to ca. 120 kg mm^{-2}) after rapid solidification, that decreased during ageing at 500 °C heat treatments (to ca. 40 kg mm^{-2}). Microhardness obtained from equiaxed microstructures indicate 15% reduction and columnar dendritic microstructures indicate 30% reduction compared to the hardness obtained from the featureless regions in rapidly solidified alloys aged at 25 °C. Microhardnesses of both dendritic and equiaxed microstructures decrease during the ageing process and the values obtained after 2 h ageing at 500 °C were ca. 45 and 30 kg mm^{-2}, respectively.

A variety of microstructures were seen principally due to local variations in the cooling rate in the ribbons [6, 5], caused by the differences in the heat transfer during the solidification process. The types of microstructures obtained after rapid solidification begun to spheroidize during the course of growth at high ageing temperatures. In our study, TEM specimens were prepared from the middle regions of the ribbons.

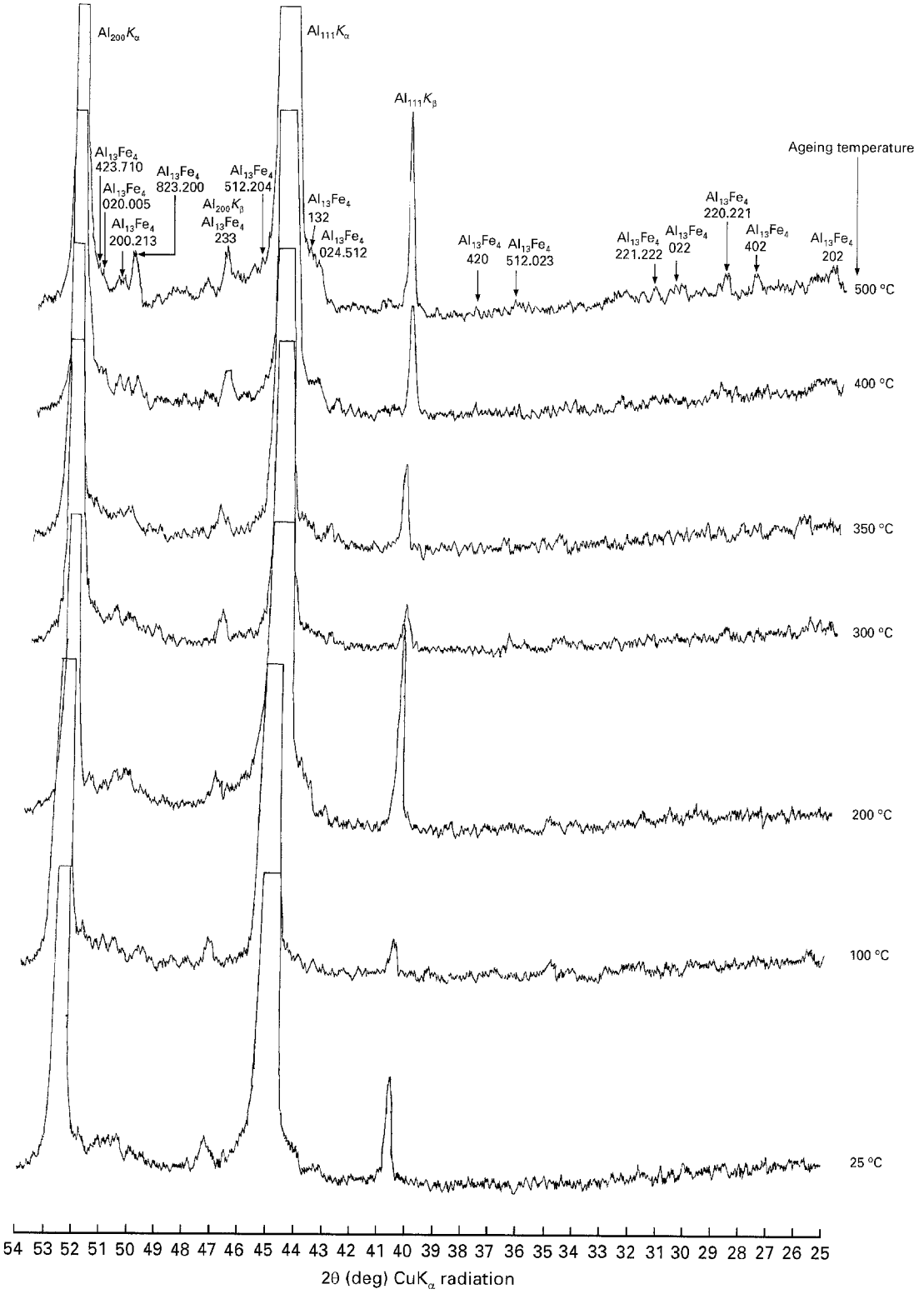

Figure 2 XRD pattern of a rapidly solidified Al–8Fe alloy after isochronal ageing at the indicated temperatures for 2 h.

In an attempt to understand the deformation mechanisms, the TEM tensile specimens were prepared and tensile tested under a microscope. The cellular dendrite type of microstructure was typical of as-cast rapidly solidified ribbons (Fig. 4). This microstructure changed during the ageing process (Fig. 5). The typical ductile transgranular fracture surfaces in rapidly solidified Al–8Fe alloys are shown in Fig. 4. The materials on either side of the crack are heavily deformed (thinned regions obtained from both sides of the crack) and the crack propagated through one of these regions precipitates, needle-like in morphology, and was broken (Fig. 4b) when the crack-tip was connected with a thinned region ahead of it. Dislocation tangle extended in front of the crack-tip (high contrast in Fig. 4b, marked by the arrow). The position of the crack and microstructure around the crack after additional straining can be seen in Fig. 4c. Crack propagation occurs within the deformed zone either by the nucleation, growth and coalescence of holes ahead of the crack-tip, or through the emission of dislocations from the crack-tip. The changes in diffraction

TABLE I d-Spacing obtained from rapidly solidified Al–8Fe alloys; XRD performed with CoK_α radiation

Phases Al	Bravais lattice $Al_{13}Fe_4$	This investigation (nm)							Reported in literature (nm)	
		As-received	Ageing temperature (°C)						Al PDS[a] 4–0787 [16]	$Al_{13}Fe_4$ PDS 29–42 [17]
			100	200	300	350	400	500		
FCC	Monoclinic									
	1 1 2		0.4252	0.4260	0.4260	0.4252				0.4258
	2 0 2		0.4063	0.4067			0.4059	0.4063		0.4064
	$\bar{2}$ 0 2, 0 2 0	0.4043	0.4039		0.4036					0.4040
	0 0 3					0.3959				0.3962
	$\bar{4}$ 0 1				0.3869					0.3872
	0 2 1	0.3826								0.3826
	4 0 0			0.3686	0.3683	0.3683		0.3670		0.3689
	$\bar{4}$ 0 2			0.3673				0.3677		0.3674
	2 2 0, $\bar{2}$ 2 1	0.3541				0.3547	0.3544	0.3544		0.3545
	0 2 2					0.3333				0.3342
	2 2 1, $\bar{2}$ 2 2		0.3269	0.3264	0.3264			0.3264		0.3268
	$\bar{4}$ 0 3		0.3232							0.3234
	$\bar{2}$ 0 4							0.3105		0.3102
	0 0 4		0.2972	0.2970		0.2976	0.2976			0.2971
	$\bar{5}$ 1 2, 0 2 3	0.2842			0.2837		0.2846	0.2842		0.2842
	4 2 0	0.2728		0.2728		0.2731	0.2731	0.2730		0.2725
	$\bar{5}$ 1 3						0.2659			0.2655
1 1 1 K_β		0.2578	0.2581	0.2581	0.2585	0.2578	0.2578	0.2581	0.2584	
	$\bar{6}$ 2 0, 3 1 3	0.2563	0.2567							0.2565
	1 3 1	0.2557	0.2557					0.2555		0.2557
	4 2 1, 5 1 1							0.2532		0.2535
	2 2 3	0.2469					0.2470			0.2469
	0 2 4, 5 1 4	0.2393	0.2393	0.2391		0.2393	0.2391	0.2394		0.2394
	1 3 2		0.2373	0.2376		0.2376	0.2376	0.2376		0.2373
	3 3 0, $\bar{1}$ 1 5					0.2369				0.2363
1 1 1 K_α		0.2335	0.2330	0.2337	0.2341	0.2333	0.2342	0.2337	0.2338	
	5 1 2, $\bar{4}$ 2 4					0.2278	0.2271	0.2278		0.2276
	$\bar{1}$ 3 3	0.2262		0.2259	0.2267	0.2267				0.2261
2 0 0 K_β		0.2234	0.2231	0.2235	0.2233	0.2233	0.2233	0.2235	0.2234	
	$\bar{3}$ 3 3		0.2175		0.2179	0.2176	0.2173	0.2173		0.2174
	1 5 5, $\bar{6}$ 2 2	0.2160	0.2159	0.2162	0.2164		0.2160	0.2160		0.2161
	$\bar{5}$ 1 5, $\bar{7}$ 1 2		0.2131	0.2129	0.2127			0.2132		0.2130
	6 2 0	0.2102	0.2103	0.2102	0.2101	0.2101	0.2102			0.2101
	$\bar{6}$ 2 3, 2 0 5	0.2098	0.2094	0.2098	0.2098	0.2094	0.2088	0.2098		0.2095
	$\bar{2}$ 0 6, $\bar{7}$ 1 3	0.2077	0.2076	0.2074	0.2080		0.2077	0.2075		0.2078
	6 0 2	0.2065				0.2060				0.2062
	0 2 5, 6 0 5	0.2050	0.2048	0.2052	0.2050	0.2052	0.2052	0.2049		0.2049
	4 2 3, 7 1 0	0.2041	0.2041			0.2041	0.2043	0.2043		0.2041
2 0 0 K_α		0.2023	0.2028	0.2023	0.2026	0.2019	0.2023	0.2023	0.2024	

[a] Powder diffraction standard.

TABLE 11 d-Spacing obtained from rapidly solidified Al–8Fe alloys; XRD performed with CuK_α radiation

Phases Al	Bravais lattice $Al_{13}Fe_4$	This investigation (nm)							Reported in literature (nm)	
		As-received	Ageing temperature (°C)						Al PDS[a] 4–0787 [16]	$Al_{13}Fe_4$ PDS 29–42 [17]
			100	200	300	350	400	500		
FCC	Monoclinic									
	1 1 2	0.4261								0.4258
	2 0 2			0.4064						0.4064
	$\bar{2}$ 0 2, 0 2 0				0.4045	0.4036	0.4038	0.4041		0.4040
	0 0 3			0.3956	0.3965	0.3969	0.3956	0.3956		0.3962
	4 0 0					0.3689	0.3685	0.3685		0.3689
	$\bar{4}$ 0 2						0.3678			0.3674
	2 2 0 $\bar{2}$ 2 1						0.3572	0.3530		0.3545
	0 2 2							0.3338		0.3342
										0.3268
	$\bar{4}$ 0 3		0.3240			0.3243	0.3240	0.3237		0.3234
	2 0 3						0.3115			0.3118
	$\bar{2}$ 0 4	0.3102								0.3102
	0 0 4					0.2976	0.2976	0.2971		0.2971
	$\bar{5}$ 1 2, 0 2 3	0.2846			0.2842		0.2842			0.2842
	4 2 0							0.2722		0.2725
1 1 1 K_β		0.2581	0.2570	0.2582	0.2601	0.2577	0.2577	0.2584	0.2584	
	$\bar{4}$ 2 3					0.2524		0.2519		0.2525
	0 2 4, $\bar{5}$ 1 4	0.2397	0.2402	0.2396	0.2393	0.2393	0.2399	0.2396		0.2394
	1 3 2	0.2379	0.2377	0.2374	0.2377		0.2374	0.2374		0.2373
	3 3 0, $\bar{1}$ 1 5	0.2362				0.2362				0.2363
1 1 1 K_α		0.2329	0.2321	0.2330	0.2342	0.2326	0.2327	0.2334	0.2338	
	$\bar{3}$ 3 2				0.2314					0.2315
	5 1 2, $\bar{4}$ 2 4		0.2273	0.2273			0.2278			0.2276
	$\bar{1}$ 3 3					0.2267	0.2269			0.2261
2 0 0 K_β		0.2231	0.2231	0.2231	0.2231	0.2230	0.2230	0.2233	0.2234	
	1 5 5, $\bar{6}$ 2 2							0.2167		0.2161
	$\bar{5}$ 1 5, $\bar{7}$ 1 3		0.2125	0.2129	0.2128	0.2128	0.2134	0.2131		0.2130
	6 2 0		0.2101	0.2101	0.2101	0.2101	0.2103	0.2103		0.2101
	$\bar{6}$ 2 3, 2 0 5	0.2098	0.2090	0.2093	0.2090	0.2088	0.2091	0.2093		0.2095
	$\bar{2}$ 0 6, $\bar{7}$ 1 3	0.2079	0.2078	0.2080	0.2076	0.2077	0.2074	0.2074		0.2078
	6 0 2	0.2068			0.2063					0.2062
	0 2 5, 6 0 5	0.2048	0.2048	0.2051	0.2050	0.2048	0.2048	0.2048		0.2049
	4 2 3, 7 1 0	0.2040	0.2040	0.2040	0.2042	0.2041	0.2041	0.2040		0.2041
	4 2 5					0.2033	0.2034			0.2031
2 0 0 K_α		0.2024	0.2019	0.2020	0.2027	0.2017	0.2019	0.2023	0.2024	

[a] Powder diffraction standard.

conditions due to local bending give new locations at the appearance of dislocation regions (high contrast in region A). While the aged specimens did not change the modes of either the fracture or the deformation during straining, there was an influence on crack propagation – the crack would pass through the matrix near the precipitates (Fig. 5a). This effect was most clearly demonstrated when the specimen was first strained and a crack was initiated (Fig. 5a), and then the additional straining caused the crack to pass in the vicinity of large precipitates (marked by the arrows). Crack propagation would not be through any one, or on the boundary, of these precipitates. A crack-tip and the microstructure formed around the crack during its advance, create a region ahead of the tip of relatively thick material that has been thinned to electron transparency by a plastic deformation process. Thickness contrast fringes are observed in the zone ahead of the crack-tip (marked by the arrows in Fig. 5b). Broadened contrast fringes in a plastic region are due to extinction contours, indicated by their diffuse appearance and extremely high dislocation density (Fig. 5b, zone A). At high magnification, the interaction between propagated crack and the single precipitate can be seen in the sample after ageing heat treatment at 500 °C (Fig. 6). The crack changes the advance direction before the precipitate (apparently lower energy needed) and propagated in the depletion zones of the matrix in the vicinity of the large precipitate. In addition, the deformation band contrasts with dense dislocation tangles ahead of the crack (Fig. 6).

Grain boundary deformation and a crack crossing a grain boundary was observed between a propagating crack and a microstructure in rapidly solidified Al–8Fe alloys (Fig. 7). The deformation band passed through the grain selecting the $\{1\,1\,1\}\langle 1\,1\,0\rangle_\gamma$ slip

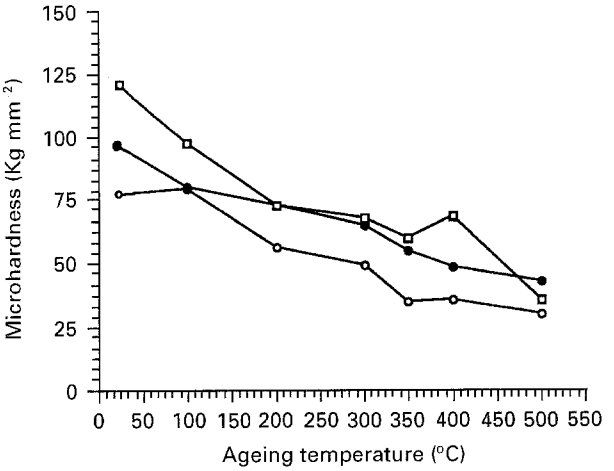

Figure 3 Knoop microhardness of a rapidly solidified Al–8Fe alloy after isochronal ageing for 2 h. ○ Equiaxed zone; ● Dendritic zone; □, Featureless zone.

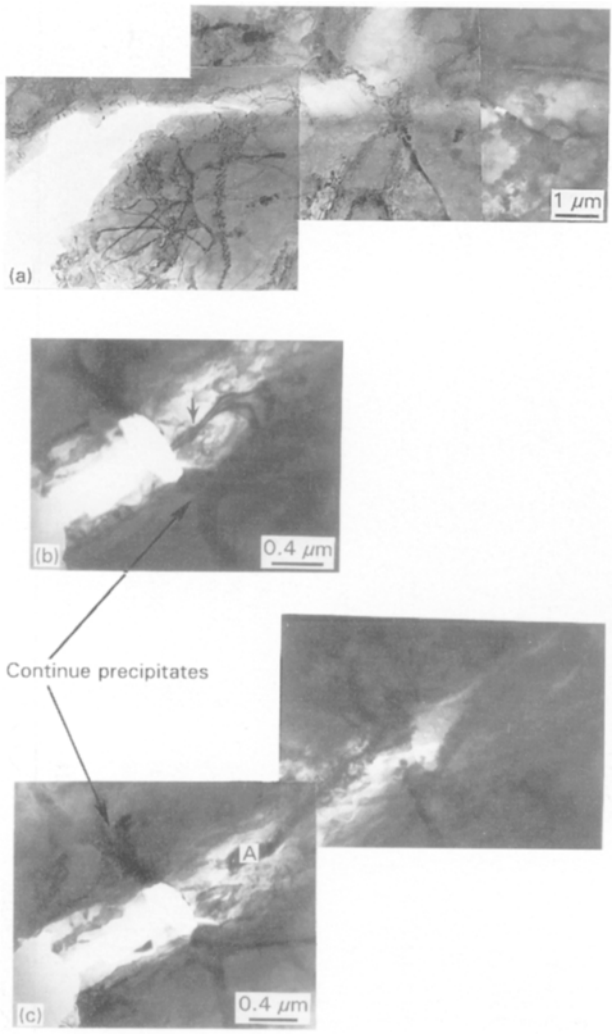

Figure 4 (a) Typical fracture surfaces obtained from a rapidly solidified as-melted Al–8Fe alloy, strained under TEM; (b) magnification of the crack-tip in the strained zone; (c) additional straining of (b).

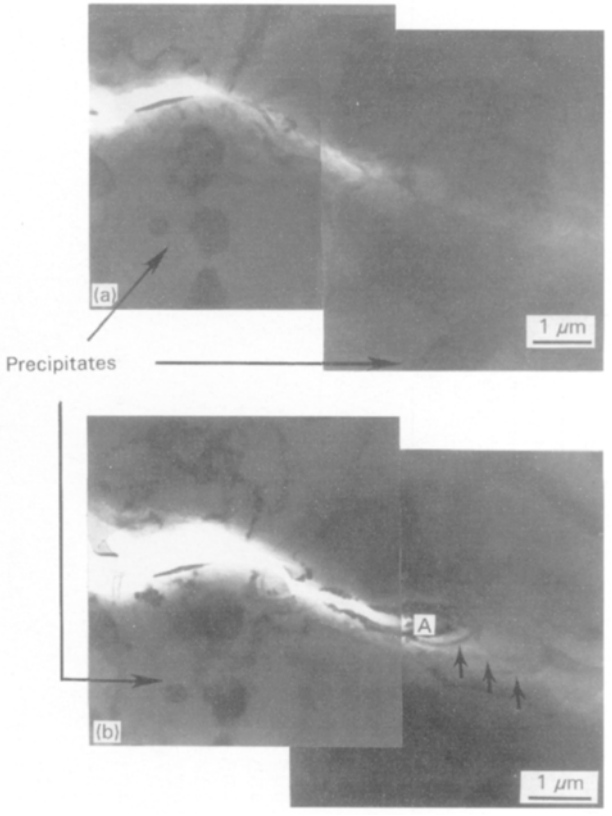

Figure 5 Typical fracture surfaces obtained from a rapidly solidified Al–8Fe alloy after 2 h ageing at 500 °C, strained under TEM. (a) Magnification of the crack-tip in the strained zone; (b) additional straining of (a).

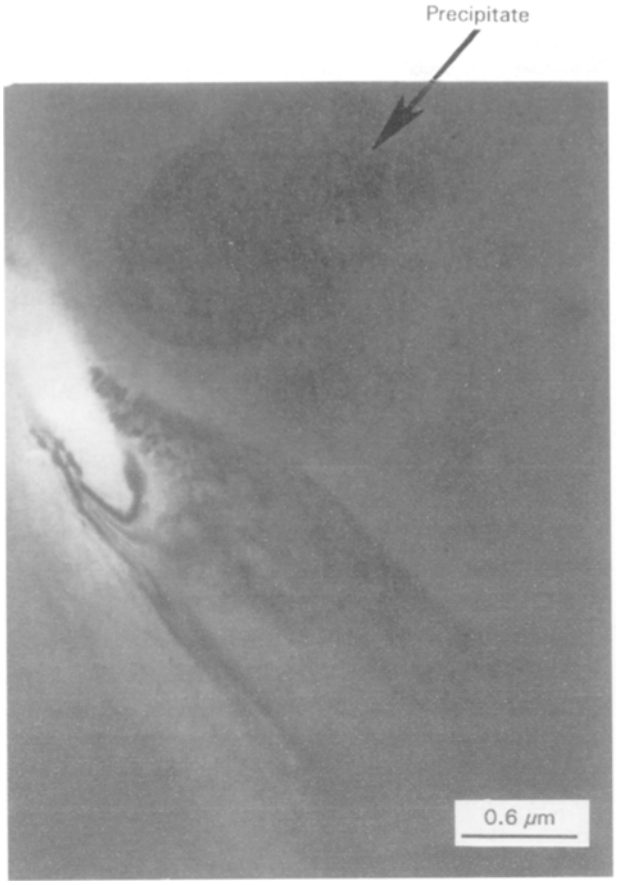

Figure 6 Microcrack and plastic thinning near coarse precipitates in an Al–8Fe alloy after 2 h ageing at 500 °C, strained under TEM.

Figure 7 Deformation crossing grain boundary in a rapidly solidified Al–8Fe alloy after isochronal ageing at 500 °C for 2 h, strained under TEM. (a) Crack blocked before the grain boundary; (b) thinning and microvoid formation in the second boundary; (c) opening of the microvoid and joining to the main crack.

Figure 7 Continued.

plane system having a maximum resolved shear stress and interacting with the grain boundary. Propagation of the crack was generally blocked before the grain boundary (Fig. 7a). The deformation band passed through the grain boundary (Fig. 7b). A microvoid formed on the other slip plane of the second grain (marked by the arrow in Fig. 7b). The opening of the microvoid (Fig. 7b) and joining to the main crack (Fig. 7c) are typical in formation of transgranular ductile fracture surfaces.

4. Discussion

Al–8Fe alloys produced by rapid solidification techniques exhibit improvement in mechanical properties at elevated temperatures. Strength and stability of these alloys depend on non-equilibrium intermetallic phases, thermal stability and impurities in the intermetallics [1–6]. Three different phases have been suggested [7–10] – tetragonal Al_4Fe, orthorhombic Al_3Fe and tenfold twins of $Al_{13}Fe_4$. By the conventional X-ray technique, it is difficult to draw the line between detected and undetected small amounts of intermetallic phases. XRD patterns from these phases were readily indexed as $Al_{13}Fe_4$ (Figs 1 and 2) and the summary of these results is given in Tables I and II. The lattice parameter of the solid solution of Al decreases during the ageing process (Figs 1 and 2). Fe in solid solutions of Al decrease the lattice parameter [11]. Coarsening of the continuous precipitates and the appearance of separate precipitates increased the diffraction intensities obtained from $Al_{13}Fe_4$ particles in the specimens after higher ageing temperatures. The reason for the appearance of new diffraction peaks from the $Al_{13}Fe_4$ phase only after a high temperature ageing process was the preferential growing of precipitates during the ageing treatments.

The fracture mechanisms are similar to those reported in other FCC ductile metals [12–14]. The fracture mode was predominantly transgranular and crack advance was preceded by a localized plastic deformation which thinned the materials ahead of the crack-tip. Large deformations were observed in front of the crack-tip, as the materials which were completely opaque electron thinned sufficiently to become electron transparent. Crack advance was confined to this deformation zone and occurred either by the direct emission of dislocations from the crack-tip or by the nucleation, growth and coalescence of holes (Figs 4–7).

The size, density and morphology of secondary phases influence crack initiation and propagation in both rapidly solidified and aged Al–8Fe alloys. TEM micrographs obtained from the columnar dendritic zone (Fig. 4) show high amounts of the continuous intermetallic phases and cracks propagated through these phases. On further straining, the crack-tip dislocation became fully incorporated with these continuous precipitates. Dislocation density increased during this incorporation process, indicating that the dislocation strain fields had also increased. No dislocations were ejected from the interface into the adjoining intermetallic phase. At the critical, but undetermined, stress level the intermetallic phase failed and the second grain relieved the accumulated stress, and crack propagation continued as described previously (Fig. 4b). The rapidly solidified specimens after ageing heat treatments showed large coarse precipitates (0.5–2 mm in diameter) with geometrical morphologies (Fig. 5). The transgranular crack propagation and the deformation mechanism processes deviate to pass in the vicinity of these large precipitates. Extensive local plastic deformation and thinning of the matrix were typical of crack propagation near the precipitates (Fig. 6). However, in the case of continuous precipitates, in microstructures under applied tensile stresses, crack propagation was through the continuous non-coherent precipitates, but in the case of rapidly solidified and aged specimens, crack propagation passed through the matrix (in the depletion regions of the matrix) in the vicinity of the precipitates.

The common interactions between the dislocation interaction and a secondary phase in both the as-received and aged rapidly solidified Al–8Fe alloys were observed. Blocking the direct passage of dislocation by the continuous and coarse precipitates, and the formation of complex tangles, led to observation of dislocation structures. Formation of high dislocation density regions were associated with high residual contrast (Figs 4 and 5), giving rise to crack initiation processes [15].

The common interaction between a propagating crack and a grain boundary in both as-received and after ageing rapidly solidified alloys was observed (Fig. 7). The deformation band passed through the grain boundary selecting the $\{1\,1\,1\}\langle 1\,1\,0\rangle_\gamma$ slip planes having a maximum resolved shear stress in the adjacent grain and interacting with the grain boundary close to the intersection of the pile-up with the grain boundary. Propagation of the crack was generally blocked before the grain boundary. A microvoid formed on the second grain (marked by an arrow in Fig. 7b). The opening of microvoids (Fig. 7c) joined to the main crack are typical of the transgranular ductile fracture surfaces.

The as-quenched microstructure of rapidly solidified Al–8Fe alloys is very heterogeneous. A variety of microstructures were seen principally due to local variation in cooling rate at various locations in the ribbon resulting from differences in heat transfer [2]. The microhardnesses obtained from Al–8Fe alloys (Fig. 3) are consistent with solidified heterogeneous structures of melt-spun alloys [5]. From the secondary phases morphology standpoint, featureless zones developed from the wheel side have the higher microhardness values [ca. 120 kg mm^{-2} (Knoop hardness)], the slightly lower hardness obtained at the dendritic zones, while the lower hardness was typical in the equiaxed zones that developed at the air size of the specimens. The melt-spun Al–8Fe alloys are dispersion and grain boundary hardened by the non-coherent intermetallic microcrystalline phases. Hardness resulting from isochronal ageing are shown in Fig. 3 for various zones of the Al–8Fe ribbons. Hardness decreases in various zones of the specimens were obtained at higher ageing temperatures. TEM results during straining clearly show that the deformation processes of thinning ahead of the crack-tip affects the microstructure, explaining the microhardness results. This work clearly shows that in order to obtain coarse intermetallic precipitates after ageing heat treatments crack propagation and deformation processes ahead of crack-tip occur at lower stresses compared to as-received rapidly solidified samples. Finally, it should be noted that the microcrystalline morphology of non-coherent structures of the secondary phases and grain boundaries have a very efficient mechanism of hindering Al–8Fe rapidly solidified alloys.

5. Conclusions

1. In the present paper a series of conclusions are drawn from the TEM fracture specimens. While these are based on observation on thin specimens they are consistent with the behaviour observed for macroscopic specimens. The most general conclusion which can be drawn is clearly in agreement with a plastic mechanism. Crack propagation occurs by localized plastic rupture mechanisms which result from enhanced slip along $\{1\,1\,1\}_\gamma$ planes. Crack propagation occurs within the deformed zone either by the nucleation, growth and coalescence of holes ahead of the crack-tip or through the emission of dislocation from the crack-tip. The resulting fracture is along the active $\{1\,1\,1\}_\gamma$ slip planes.

2. The principal effect of the secondary phase ($Al_{13}Fe_4$) on fracture propagation in Al–8Fe alloys is that they increase the stress at which plastic deformation occurs at the crack-tip and thereby the stress at which the crack propagates.

3. This work clearly shows that in order to obtain coarse intermetallic precipitates in the specimens after ageing heat treatments, the crack propagation and deformation processes are possible by low stress levels compared to as-received rapidly solidified samples.

References

1. H. JONES, *Aluminium* **54** (1978) 274.
2. *Idem., Mater. Sci. Engng.* **65** (1984) 145.
3. C. C. KOCH, *Int. Mater. Rev.* **33** (1988) 201.
4. R. A. DUNLAP, D. J. LLOYD, I. A. CHRISTIE, G. STROINK and Z. M. STADNIK, *J. Phys. F. Met. Phys.* **18** (1988) 1329.
5. S. J. SAVAGE and F.H. FROES, *J. Metals* **36** (1984) 20.
6. H. JONES, *Mater. Sci. Engng.* **5** (1969) 1.
7. R. WANG, J. GUI, S. YAO, Y. CHEN, G. LU and M. HUANG, *Phil. Mag. Lett.* **54** (1986) L 33.
8. S. SRIRAN and J. A. SEKHAN, *Mater. Sci. Engng.* **66** (1984) L 9.
9. A. K. GOGIA, P. V. RAO and J. A. SEKHAR, *J. Mater. Sci.* **20** (1985) 3091.
10. M. CHANDRASEKARAN, Y. P. LIN, R. VINCENT and G. STANIEK, *Scripta Metall.* **22** (1988) 797.
11. H. JONES, *ibid.* **17** (1983) 97.
12. H. G. F. WILSDORF, *Acta Metall.* **30** (1982) 1247.
13. G. M. BOND, M. ROBERTSON and H. K. BIRNBAUM, *ibid.* **35** (1987) 2289.
14. P. ROZENAK, *Mater. Sci. Engng.* A **128** (1990) 91.
15. P. ROZENAK, *J. Mater. Sci. Lett.* **9** (1990) 177.
16. "Powder Diffraction File", Joint Commitee on Powder Diffraction Standards, Swarthmore, PA, 1979, **4**.
17. *Idem.*, Swarthmore, PA, 1979, **29**.

Received 25 October 1994
and accepted 13 February 1996